Growth and microstructure dependence of electronic and magnetic properties in magnetically doped Gd-Si amorphous semiconductors

Li Zeng
Materials Science and Engineering Program, University of California, San Diego, La Jolla, California 92093, USA and Department of Materials Science and Engineering, University of California, Berkeley, Berkeley, California 94720, USA

Erik Helgren and Frances Hellman
Department of Physics, University of California, Berkeley, Berkeley, California 94720, USA

Rafiqul Islam and David J. Smith
Center for Solid State Science, Arizona State University, Tempe, Arizona 85287, USA and Department of Physics and Astronomy, Arizona State University, Tempe, Arizona 85287, USA
(Received 1 July 2006; revised manuscript received 11 December 2006; published 4 May 2007)

A comparision of the electronic and magnetic properties of amorphous Gd_xSi_{1-x} (a-Gd-Si) thin-film alloys prepared by different growth techniques (e-beam evaporation and magnetron sputtering) is reported. High-resolution cross-sectional transmission electron microscopy (HR-XTEM) and Rutherford backscattering (RBS) show that the material microstructure is highly dependent on deposition method and growth conditions. Electron-beam-evaporated films have columnar microstructure (column width ~10 nm) while magnetron-sputtered films prepared at low argon partial pressure are featureless. However, the dc conductivity, magnetoresistance, and $M(H,T)$ properties of the films are totally *independent* of this difference in microstructure at the length scale of 10 nm. RBS shows that the films have the same overall atomic number density, independent of Gd incorporation, for a wide range of doping concentrations (up to 18 at. %), and HR-XTEM shows a dense, homogenous, and amorphous phase with no clustering at the atomic level. The independence of properties from the nanoscale microstructure strongly argues that the magnetic moment and charge carrier behavior observed previously are a result of fundamental interactions at the atomic level. Films sputtered at high argon pressure are less dense and have an open columnar microstructure which leads to fast degradation of film properties due to massive bulk oxidation.

DOI: 10.1103/PhysRevB.75.184404 PACS number(s): 75.50.Pp, 68.55.−a, 71.23.Cq, 71.30.+h

I. INTRODUCTION

Magnetic rare-earth-doped amorphous semiconductors have strong magnetic moment and carrier interactions, which lead to remarkable magnetic, transport, and magnetotransport properties. Previous studies documenting amorphous Gd_xSi_{1-x} (a-Gd-Si) films prepared by e-beam coevaporation can be found in the literature.[1–4] In these amorphous films, Gd acts as a trivalent magnetic dopant with a half-filled f electron shell. Gd provides both transport electrons and a large local magnetic moment, $J=S=7/2$, in the amorphous semiconductor matrix. This combination of high carrier density and large magnetic moment concentration has significant consequences for the electronic properties, including a concentration and magnetic-field-tuned metal-insulator (M-I) transition,[1] a concentration-dependent characteristic temperature[2] (T^*) at which the interactions between local moments and electrons turn on (leading to enormous magnetoresistance below T^*),[3] and universal concentration and magnetic-field-tuned scaling of the M-I quantum phase transition.[4] There are strong similarities between this system and the widely studied dilute magnetic semiconductors (DMSs), such as $Ga_{1-x}Mn_xAs$ and the perovskite manganites. In all of these systems, there is evidence for interactions between the magnetic dopants and the charge carriers. Moreover, coupling between the intrinsic positional disorder of the magnetic dopant and the crystalline lattice structure of the matrix has been suggested to play an important role in the DMS systems. Amorphous Gd-Si films have a large structural disorder compared to their crystalline counterparts.

Whether these electronic properties are associated with the specific microstructure of the amorphous matrix is unknown. Quantitative theoretical descriptions of the highly disordered amorphous materials are not as well defined as their crystalline counterparts due to the loss of periodic structure. As with crystalline materials, a complete description and understanding of the physical properties of the amorphous material ultimately depends on knowledge of the structure. Being amorphous, the films can exhibit a wide variety of short-range order and nanoscale microstructure, which could lead to distinctive physical properties. The atomic-level arrangement, microstructure, and thus often the film properties are strongly dependent on deposition methods and conditions.

Electron-beam (e-beam) evaporation and magnetron sputtering are two widely used and very different deposition methods in thin-film technology. One of the major differences between the two is the incident energy of adatoms and the consequent growth kinetics. For e-beam evaporation, the kinetic energy of adatoms is obtained from the thermal energy at the evaporation source, usually a fraction of 1 eV. For magnetron sputtering, the kinetic energy is obtained from momentum transfer between the high-energy working-gas atoms (usually Ar atoms with hundreds of eV) and the

 ©2007 The American Physical Society

target atoms. The sputtered target atoms usually have initial kinetic energy of ~10–50 eV, and the reflected neutral Ar atoms also have significant energy.[5,6] These high-energy atoms play an important role in compacting the film as it grows, under the condition that they can reach the substrate without significant energy loss due to thermal collisions with the background gas species. The kinetic energy of these atoms can be reduced by increasing the background pressure. This provides magnetron sputtering with a significant control parameter: namely, the background gas pressure. At low substrate temperature, meaning low compared to the melting temperature (T_m) of the deposited materials [for most metal and semiconductor materials, room temperature (RT) is sufficiently low], *e*-beam-evaporated films including amorphous alloys usually have columnar microstructure associated with tensile stress.[7,8] The more energetic adatoms in magnetron sputtering have more surface mobility, which helps to relax the tensile stress typically observed in thermally evaporated films grown on substrates at low temperature. At low argon pressure, when the energetic sputtered target atoms reach the substrate without significant thermalizing from gas-phase collisions, large compressive stress is found. A transition from compressive to tensile stress with increasing argon pressure has been reported in many sputtered material systems, associated with increasing thermalization of the energetic atoms.[9–14]

For the magnetically doped amorphous semiconductor system studied here, the atomic environment is key to understanding the underlying physical properties. In particular, it is crucial to understand whether the remarkable magnetic and magnetotransport properties are dependent on microstructural details. In this work, we prepared *a*-Gd-Si films by magnetron sputtering at different argon pressures, which lead to different film microstructures. We report the transport and magnetic properties of the sputtered films and directly compare them to films prepared by *e*-beam evaporation. Our effort is aimed at reproducing the unique electronic and magnetic properties of *e*-beam-evaporated *a*-Gd-Si films by optimizing the sputtering growth conditions and also to investigate whether differences in microstructure of the sputtered films will limit the reproducibility of these material properties.

II. EXPERIMENT DETAILS

Details regarding the preparation of the *e*-beam-evaporated films have been described previously.[15] The magnetron-sputtered *a*-Gd-Si films were prepared in an AJA magnetron sputtering system by cosputtering from individual high-purity Gd and Si targets. The base pressure prior to deposition was better than 8×10^{-8} Torr with a liquid-nitrogen cold trap. Films were sputtered at two different argon pressures: 2 mTorr and 6 mTorr. Within each set, one film was capped with a 250-Å amorphous Si (*a*-Si) layer. The electrical conductance was checked as a function of time after removal from the vacuum to test for film stability. The film composition and areal density (atoms/cm^2) were measured by Rutherford backscattering (RBS). Together with film thickness as determined via a Nanopics atomic force microscopy (AFM) profilometer, we extracted the atomic number density (atoms/cm^3) of the films. High-resolution cross-sectional transmission electron microscopy (HR-XTEM) and energy-dispersive spectroscopy (EDS) were used to assess the film microstructure and to verify film composition. The impurity level, specifically the oxygen content, was analyzed using oxygen-resonance RBS spectra. The temperature and magnetic field dependence of electrical transport, magnetotransport, and magnetization were measured. Further details about the experiment setups are described elsewhere.[1,15,16]

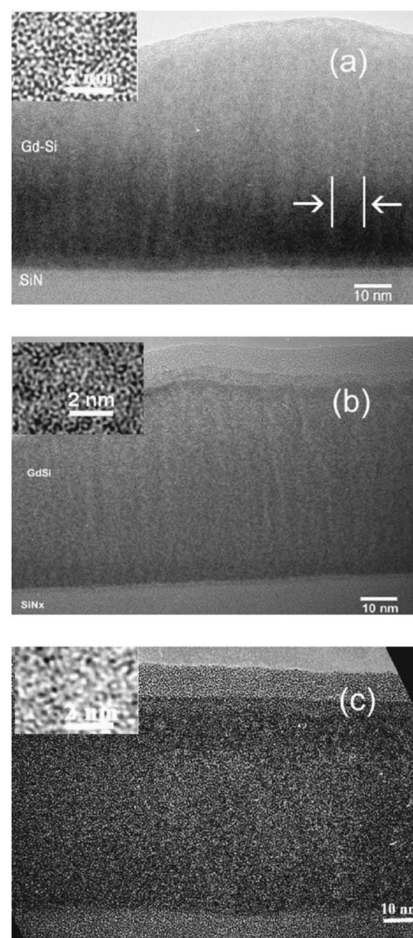

FIG. 1. XTEM micrographs for an (a) *e*-beam-evaporated sample, (b) sputtered sample prepared at 2 mTorr, and (c) sputtered sample prepared at 6 mTorr. Note the differences in film morphology. Insets for each are HR-XTEM micrographs.

III. MATERIAL AND STRUCTURAL CHARACTERIZATION

A low-magnification XTEM micrograph for an *e*-beam-evaporated film [Fig. 1(a)] shows columnar nanoscale microstructure with an average column diameter of ~10 nm. Low-magnification XTEM micrographs for the sputtered films show quite different microstructure, depending on the sputtering pressure. The film sputtered at 2 mTorr does not show columnar microstructure [Fig. 1(b)]: instead,

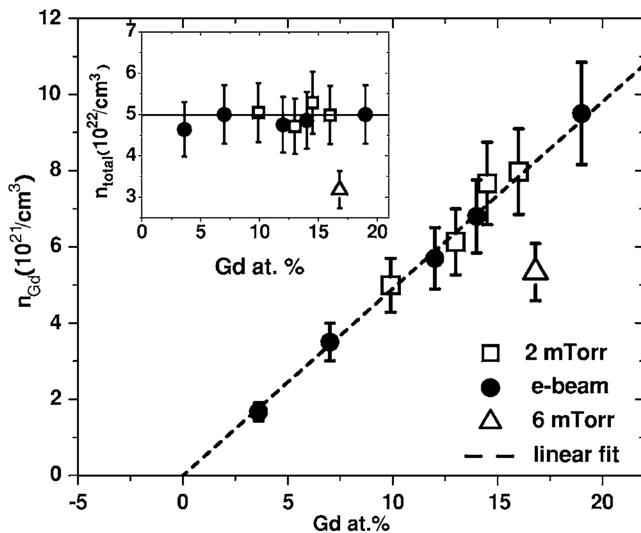

FIG. 2. Gd atomic density as function of Gd concentration. The inset shows overall atomic densities of the films in atoms/cm^3. The atomic density of pure (crystalline) silicon (4.99×10^{22} atoms/cm^3) is marked as a straight line. For reference, the bulk density of pure gadolinium is 3.01×10^{22} atoms/cm^3.

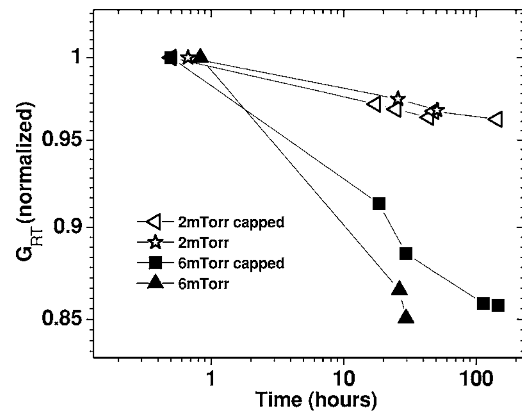

FIG. 3. Plot of conductance at room temperature (G_{RT}) vs time for different samples under ambient conditions. Data are normalized to the first measured value for each sample.

the film morphology appears featureless and homogenous. The film sputtered at 6 mTorr [Fig. 1(c)] shows columnar nanoscale microstructure with an average column diameter also of ~10 nm. At high resolution, the HR-XTEM micrographs in the insets of Fig. 1 show that the atomic microstructure for all of the films is featureless and amorphous, despite the differences in the nanoscale microstructure.

Figure 2 shows a plot of the Gd atomic number density n_{Gd} as a function of Gd concentration x. The results for the e-beam-evaporated and sputtered 2 mTorr films are identical. A linear fit of the data yields a slope of $(4.90 \pm 0.07) \times 10^{22}$ atoms/cm^3. This is the total number density n_{total} (including both Gd and Si atoms) of the a-Gd-Si films, 1.8% less dense than pure crystalline Si (4.99×10^{22} atoms/cm^3 at 300 K), but consistent with the measured number density of a-Si films prepared either by e-beam evaporation[17] or by self-ion implantation of crystalline Si (c-Si).[18] The film sputtered at 6 mTorr has a ~35% lower Gd number density for the same Gd concentration x (as shown in Fig. 2). The inset of Fig. 2 shows the total atomic number density n_{total} vs x. For a wide range of Gd doping concentrations, n_{total} is independent of x for both the e-beam-evaporated films and the sputtered 2-mTorr films. The n_{total} for the sputtered 6-mTorr film is ~35% below the value for pure a-Si.

The atomic number density result for the e-beam-evaporated films is consistent with the previous x-ray absorption fine structure (XAFS) study.[19] In the XAFS study, the average Si-Si distance was shown to be 2.39 Å, only slightly larger (by ~0.04 Å) than the Si-Si bonding distance measured in pure c-Si or a-Si. The Si-Si coordination number was measured to be 3.7, in excellent agreement with values found for a-Si prepared by self-ion implantation of c-Si and measured by a high-resolution radial distribution function (RDF).[20] The average Gd-Si distance was found to be 2.98 Å. All of these values are independent of x, from low Gd concentration up to at least $x=18$ at. %, which is in good agreement with the invariant film total number density n_{total}. The large Gd-Si distance found by XAFS indicates severe distortion of the a-Si matrix near the Gd atoms.[19] However, strain caused by the distortion is strongly localized near the Gd atoms, since both the average Si-Si bonding distance and the coordination number remain the same as for pure a-Si, implying that the amorphous Si structure is highly effective in relaxing local strain.

The identical and invariant total atomic number densities for both e-beam-evaporated and sputtered 2-mTorr films indicate that they share the same local environment envisioned as the following: each Gd ion is substituted for a single Si atom in the a-Si matrix, with very little structural expansion, despite the significant differences in ionic and covalent radii. Conceptually, starting with a pure a-Si structure, one Si atom is replaced with one Gd ion, expanding the first Si coordination shell (large Gd-Si distance measured by XAFS) in order to accommodate the larger ionic size of Gd. However, the second Si coordination shell remains almost unaffected, except for an increase of mean-square disorder of the Si-Si interatomic distance, as discussed by Haskel *et al.*[19]

Room-temperature dc conductance (G_{RT}) and the conductance ratio between RT and 77 K ($G_{RT}/G_{77\text{ K}}$) can be used as benchmarks to monitor the structure stability under ambient conditions. The G_{RT} values of the a-Gd-Si films sputtered at 2 mTorr and those grown by e-beam evaporation are stable over time (including after a number of years for the latter material) even with no capping layer. For the sputtered film prepared at 2-mTorr argon pressure, G_{RT} changes by less than 5% over 100 h (as shown in Fig. 3) and the $G_{RT}/G_{77\text{ K}}$ ratio changes less than 1.5% for a wide range of film composition and film thickness. The relatively constant values of $G_{RT}/G_{77\text{ K}}$ suggest that the change in G_{RT} is due to simple geometric changes in the conduction path (such as film thickness or volume reduction), an effect previously seen in annealing studies of a-Nb-Si.[21] The slight reduction of conductance over time is very likely due to a self-limiting thin oxidation surface layer, as observed in films prepared by e-beam evaporation when this native oxide was used to provide a controllable tunnel barrier for Pb counterelectrodes.[22] Further evidence for the self-limiting oxide comes from the

fact that no oxygen was detected in the bulk of the film by RBS oxygen-resonance spectra.

In comparison, films prepared at 6 mTorr show dramatic relaxation of material structure when exposed to air. The G_{RT} is reduced by ~15% over a period of 30 h, as shown in Fig. 3. A 250-Å *a*-Si capping layer (sputtered also at 6 mTorr) does not prevent this relaxation. On the other hand, the $G_{RT}/G_{77\ K}$ ratio shows no significant change. RBS and EDS analyses both show significant oxygen content in the films. The degradation of films prepared at 6 mTorr is thus likely to be due to formation of insulating oxides within the film. For sputtered metal films, the microstructure obtained at high sputtering pressures is characterized by tapered crystals separated by open, voided boundaries; these porous boundaries serve as fast diffusion paths leading to massive bulk oxidation.[11,13,14] Although this zone model was originally proposed for sputtered metal films with polycrystalline structure, similar sputtering pressure dependence of the film microstructure and impurity level has also been found for sputtered amorphous alloys, such as Tb-Fe,[12] TaB_x, and $TaSi_x$.[23] The lower overall number density for the sputtered 6-mTorr films indicates a less dense, open columnar structure. It is interesting to note that our *e*-beam *a*-Gd-Si films have an apparently similar columnar microstructure (as seen in the XTEM micrograph in Fig. 1), but do not show any oxygen from RBS or degradation of the film properties. We suggest therefore that the substantial differences in the stability of the material electronic properties are linked specifically to changes in atomic structure (measured by the average atomic number density), which is more significant than the columnar nanoscale microstructure.

IV. ELECTRONIC AND MAGNETIC PROPERTIES

Figure 4 shows the dc conductivity $\sigma_{dc}(T)$ of the *a*-Gd_xSi_{1-x} films sputtered at 2 mTorr for various Gd concentration x. The monotonic increase of the $\sigma_{dc}(T)$ curves with respect to the Gd doping concentration x indicates the successful electrical doping behavior of Gd in the *a*-Si as matrix, previously seen for *e*-beam-evaporated samples. As x spans between 9.9 and 18.0 at. %, the system undergoes a concentration-driven *M-I* transition at a critical concentration $x_c \sim 14.5$ at. %, as shown in Fig. 4(a). In *M-I* transition physics, a metal is defined as its residual dc conductivity at $T \to 0$ K is finite while an insulator is defined as its residual conductivity at $T \to 0$ K is zero. The sputtered *a*-$Gd_{0.145}Si$ is very slightly on the insulating side of the *M-I* transition, whereas the *M-I* transition for the *e*-beam films is at $x_c = 14.0$ at. %, suggesting a small shift in the critical concentration. However, this difference is close to the compositional resolution of RBS and may not be meaningful. Figure 4(b) shows a direct comparison of two sputtered and two *e*-beam-evaporated films: for similar compositions, $\sigma_{dc}(T)$ is nearly identical.

Figure 5 shows $\sigma_{dc}(T)$ for *a*-$Gd_{14.5}Si$ sputtered at 2 mTorr in various magnetic fields at low temperature. As previously seen for *e*-beam-evaporated films, there is a very large negative magnetoresistance (MR), due to interactions between the magnetic moments and the conduction electrons. The fact that the MR stays the same even with different microstructure as compared to the *e*-beam samples is profoundly important and indicates the unimportance of structure on the 10-nm scale.

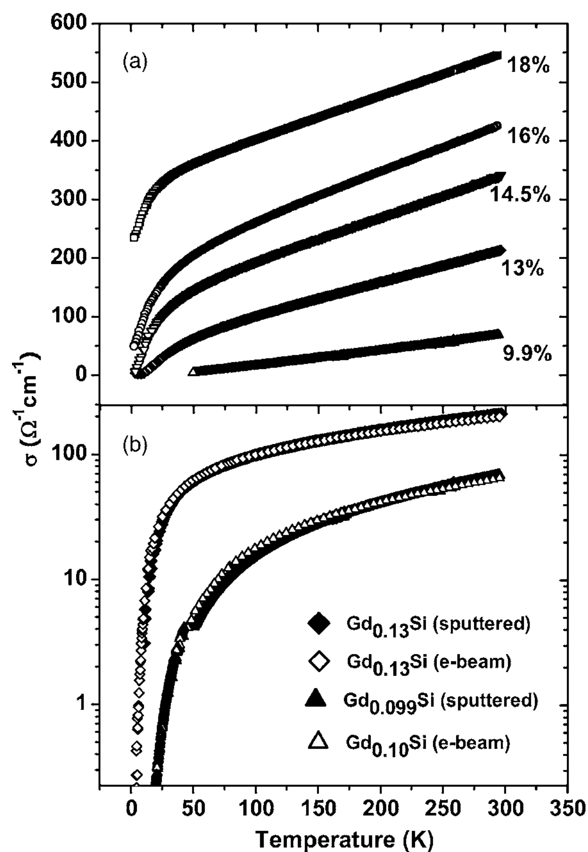

FIG. 4. (a) $\sigma_{dc}(T)$ for sputtered *a*-Gd-Si prepared at 2 mTorr with different Gd concentrations. The 14.5 at. % sample is just on the insulating side of the *M-I* transition. (b) $\sigma_{dc}(T)$ for two sputtered samples prepared at 2 mTorr overlayed on data for *e*-beam-evaporated samples.

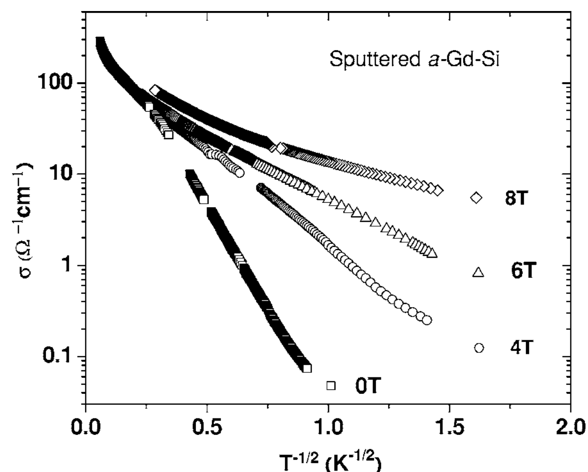

FIG. 5. $\sigma_{dc}(H,T)$ plotted vs $T^{1/2}$ for a 14.5 at. % sputtered *a*-Gd-Si sample prepared at 2 mTorr for $H=0,4,6,8$ T. A very large negative MR is seen in these sputtered samples similar to previously measured *e*-beam samples (Ref. 16).

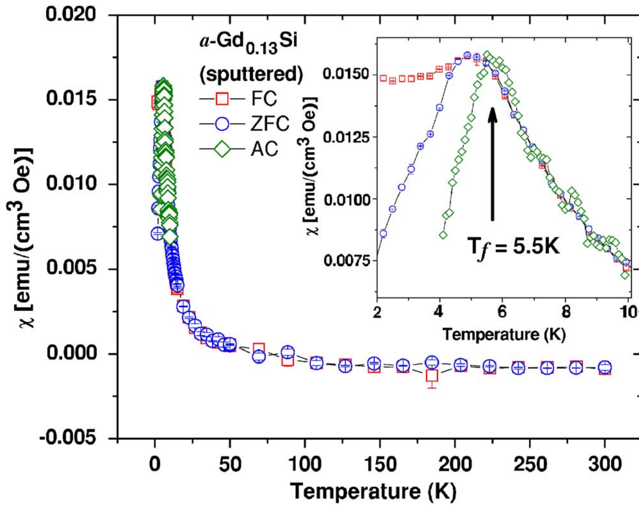

FIG. 6. (Color online) ac and dc susceptibility for a 13 at. % sputtered a-Gd-Si sample prepared at 2 mTorr. dc data measured at 100 Oe after cooling in zero field (ZFC) or on cooling in 100 Oe (FC). ac data measured in a 4-Oe, 135-Hz oscillating magnetic field.

Zero-field-cooled (ZFC), field-cooled (FC), and ac magnetic susceptibility $\chi(T)$ data for a 13.0 at. % sputtered film prepared at 2 mTorr are shown in Fig. 6. The ZFC and FC data were each measured in 100 Oe, after cooling in 0 or 100 Oe fields, respectively. The ac $\chi(T)$ data were measured in a 4-Oe, 135-Hz oscillating magnetic field. Previous work on e-beam-evaporated films (including frequency-dependent measurements) has established that spin-glass freezing occurs at low temperature.[15] The data for samples sputtered at 2 mTorr show the same split between ZFC and FC, and a sharp peak in ac $\chi(T)$, as for the e-beam-evaporated films. The T_f is precisely determined by the sharp peak in the ac susceptibility data for the 13 at. % sample and estimated from the splitting temperature between the ZFC and FC dc susceptibility data for the 14.5 at. % sample.

We plot the concentration dependence of T_f of the sputtered 2-mTorr samples together with the e-beam samples in Fig. 7(a). The magnitude and concentration dependence of T_f for the sputtered samples is very close to that of the e-beam-evaporated samples. T_f increases smoothly with Gd doping across the M-I transiton, indicating stronger interactions between the Gd moments. This is consistent with the decreasing Gd-Gd spacing. We note that the temperature dependence of the dc conductivity does not show any transition across T_f. The lack of features in σ_{dc} is due to no peridocially ordered spin states below the freezing temperature, and the frozen disorder is still the major mechanism for local-moment and conduction-electron scattering. Applying a small magnetic field will "melt" the spin-glass state and increase the sample conductivity, leading to large negative MR as mentioned previously. However, the characteristic temperature T^* (~75 K for a 14.0 at. % Gd sample), which is defined as temperature where the magnetoconductance (MG) equals 1% for a metallic sample,[2] is much higher than T_f, indicating that strong moment-carrier interactions appear well above the spin-glass freezing temperature. In this work,

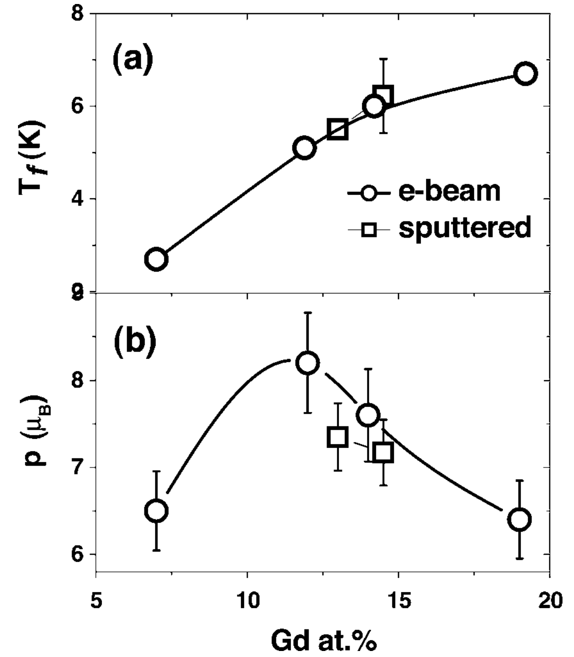

FIG. 7. (a) T_f vs Gd at. % for e-beam-evaporated and sputtered (2 mTorr) samples. T_f shown without error bar is determined by the peak in the ac susceptibility measurement. T_f shown with error bar is estimated from the splitting between the ZFC and FC dc susceptibilities. (b) Effective Gd moment from Curie-Weiss fitting vs Gd at. %.

by comparing the e-beam-evaporated and magnetron-sputtered samples, we have shown that this amazingly high characteristic temperature is *not* particularly associated with the 10-nm scale columnar microstructure only found in the e-beam evaporated samples.

In the paramagnetic state above the T_f, $\chi(T)$ fitted well with the Curie-Weiss law $\left(\chi=\frac{A}{T-\theta}\right)$ with Curie-Weiss temperature $\theta \sim 0$ K, as previously found for e-beam-evaporated films, indicating a high degree of frustration and very small net Gd-Gd interaction. The Gd effective moments p (extracted from $A=n_{\mathrm{Gd}}p^2\mu_B^2/3k_B$) also agree with the values of the e-beam-evaporated films, as shown in Fig. 7(b). The effective moment has a nonmonotonic dependence on Gd concentration, showing a peak near the M-I transition with values close to the free Gd moment. Away from the M-I transition, p drops significantly, showing suppression of the Gd local moment. Figure 8 shows that in M vs H measurements at $T=2$ K and 10 K, the moment of the 13 at. % sample sputtered at 2 mTorr ($T_f=5.5$ K) is strongly suppressed below the Brillouin function, indicating that the sample is not simply paramagnetic and has large antiferromagnetic interactions which are balanced with equally strong ferromagnetic interactions (leading to very small θ). This can be explained by RKKY interactions between the Gd moments, which have been observed in metallic Gd and $GdSi_2$ samples. Disorder will not dampen the strength of the RKKY interaction and presumably only ramdomizes the phase of the interaction. Again, the same exact effects were observed in e-beam-evaporated films.[3] The sputtered films thus behave magnetically the same as the e-beam-evaporated films; i.e.,

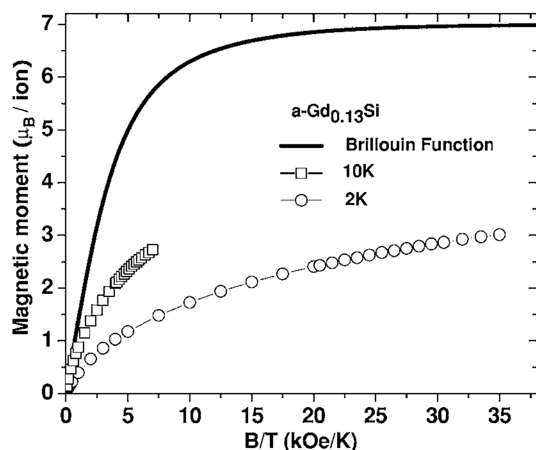

FIG. 8. The magnetization data of a 13 at. % sputtered (2 mTorr) sample are suppressed below the Brillouin function at 7 T, for temperatures both below ($T=2$ K) and above ($T=10$ K) the spin-glass freezing temperature, which is 5.5 K for this sample.

they are true spin glasses with indirect RKKY-like Gd-Gd interactions.

V. CONCLUSION

The dramatic magnetoelectronic properties previously observed for *a*-Gd-Si prepared by *e*-beam evaporation are also found in films prepared by sputtering at low argon pressure (2 mTorr), despite very different microstructure at the 10-nm scale (columnar versus dense and featureless). The magnetoelectronic properties are nearly identical, including concentration and field-tuned *M-I* transition, large negative MR, spin-glass freezing, and an anomalous effective moment with a peak near the *M-I* transition. The independence of the unique magnetic and electronic properties of the film morphology at the 10-nm scale, though perhaps expected, is experimentally clearly demonstrated. The *e*-beam-evaporated films and the sputtered films prepared at 2 mTorr have the same total atomic number density as pure *a*-Si. High-resolution cross-sectional TEM micrographs show that at the atomic level the films are amorphous with no clustering or inhomogeneity. Based on XAFS and the measured atomic number density, we propose that the atomic environment of Gd atoms consists of a highly strained first Si coordination shell embedded in a largely relaxed *a*-Si matrix. This argues that in this magnetically doped amorphous semiconductor, the strong moment-carrier interaction (which leads to large MR and T^*) and strong moment-carrier-moment interaction (RKKY-like leading to spin-glass freezing) are *only* dependent on the local atomic environment around the Gd atoms, which is therefore both intrinsic and fundamental. For the sputtered *a*-Gd-Si films prepared at 6 mTorr, low atomic density and open columnar microstructure lead to massive oxidation of the films and significant degradation of the film properties over time.

ACKNOWLEDGMENTS

We thank K.M. Yu for useful discussions and assistance with the RBS data. We acknowledge the use of facilities in the John M. Cowley Center for High Resolution Electron Microscopy at Arizona State University. This Research was supported by NSF Grants Nos. DMR-0505524 and DMR-0203907.

[1] W. Teizer, F. Hellman, and R. C. Dynes, Solid State Commun. **114**, 81 (2000).
[2] E. Helgren, J. J. Cherry, L. Zeng, and F. Hellman, Phys. Rev. B **71**, 113203 (2005).
[3] F. Hellman, M. Q. Tran, A. E. Gebala, E. M. Wilcox, and R. C. Dynes, Phys. Rev. Lett. **77**, 4652 (1996).
[4] E. Helgren, L. Zeng, K. Burch, D. Basov, and F. Hellman, Phys. Rev. B **73**, 155201 (2006).
[5] P. F. Carcia, S. I. Shah, and W. B. Zeper, Appl. Phys. Lett. **56**, 2345 (1990).
[6] H. Matsui, H. Toyoda, and H. Sugai, J. Vac. Sci. Technol. A **23**, 671 (2005).
[7] M. Ohring, *The Materials Science of Thin Film*, 1st ed. (Academic Press, New York, 1991), p. 228.
[8] M. Moske and K. Samwer, Z. Phys. B: Condens. Matter **77**, 3 (1989).
[9] J. A. Thornton and D. W. Hoffman, J. Vac. Sci. Technol. **18**, 203 (1981).
[10] D. W. Hoffman and J. A. Thornton, J. Vac. Sci. Technol. **20**, 355 (1982).
[11] J. A. Thornton and D. W. Hoffman, Thin Solid Films **171**, 5 (1989).
[12] F. Hellman and E. M. Gyorgy, Phys. Rev. Lett. **68**, 1391 (1992).
[13] A. Misra and M. Nastasi, J. Mater. Res. **14**, 4466 (1999).
[14] A. Misra and M. Nastasi, J. Vac. Sci. Technol. A **18**, 2517 (2000).
[15] F. Hellman, D. R. Queen, R. M. Potok, and B. L. Zink, Phys. Rev. Lett. **84**, 5411 (2000).
[16] P. Xiong, B. L. Zink, S. I. Applebaum, F. Hellman, and R. C. Dynes, Phys. Rev. B **59**, R3929 (1999).
[17] M. H. Brodsky, D. Kaplan, and J. F. Ziegler, Appl. Phys. Lett. **21**, 305 (1972).
[18] J. S. Custer, M. O. Thompson, D. C. Jacobson, J. M. Poate, S. Roorda, and W. C. Sinke, Appl. Phys. Lett. **64**, 437 (1994).
[19] D. Haskel, J. W. Freeland, J. Cross, R. Winarski, M. Newville, and F. Hellman, Phys. Rev. B **67**, 115207 (2003).
[20] K. Laaziri, S. Kycia, S. Roorda, M. Chicoine, J. L. Robertson, J. Wang, and S. C. Moss, Phys. Rev. Lett. **82**, 3460 (1999).
[21] D. Querlioz, E. Helgren, D. R. Queen, F. Hellman, R. Islam, and D. J. Smith, Appl. Phys. Lett. **87**, 221901 (2005).
[22] W. Teizer, F. Hellman, and R. C. Dynes, Phys. Rev. Lett. **85**, 848 (2000).
[23] K. Racette, C. Brooks, C. R. Guarnieri, and D. Hendy, J. Vac. Sci. Technol. A **18**, 1119 (2000).